Desalination and Water Treatment
www.deswater.com
doi: 10.5004/dwt.2022.28320

255 (2022) 47–55
April

Numerical simulation of flow through porous membranes with finger-like formations

Bahadir Mert Erdugan, Elif Demirel*

Department of Chemical Engineering, Faculty of Engineering, Eskisehir Technical University, 26555 Eskisehir, Turkey, Tel. +90 222 321 3550/6509; emails: elifyildiz@eskisehir.edu.tr (E. Demirel), bahadirmerterdugan@eskisehir.edu.tr (B.M. Erdugan)

Received 30 July 2021; Accepted 9 February 2022

ABSTRACT

In this study, a polyvinyl chloride based ultrafiltration membrane was fabricated through phase inversion technique and water flux was measured using a dead-end ultrafiltration system at various transmembrane pressures ranging from 0.07 to 0.27 MPa. The cross-sectional morphologies of membranes were visualized using scanning electron microscopy (SEM) to further analyze the alignment of finger-like pores based on image processing. A numerical model is developed and validated for the simulation of laminar flow through the membrane under different conditions of membrane porosity and transmembrane pressure. While the rigid pore assumption used in the numerical model gives accurate results for low pressures, the numerical model suffers from the low accuracy for high pressures since pore structure is subjected to significant compaction at high pressures. Finger-like structures were extracted from the SEM images using an image processing software and implemented to the validated numerical model in order to examine the effect of finger-like formations on the structure of membrane flow. Numerical simulation results show that a complex flow structure is formed between finger-like formations due to a strong momentum exchange between neighboring finger-like structures. Internal flow in the membrane zone is significantly influenced by the existence of finger-like formations resulting in recirculation effects and dead zones, which may lead to diminution of flux performance of the membrane. The proposed model can be further used for the investigation of optimum porosity and transmembrane pressure to enhance flux performance.

Keywords: Ultrafiltration membrane; Porous zone; Viscous flow; Numerical modelling

1. Introduction

In recent years, ultrafiltration (UF) membranes have a wide range of applications in several industries including water and wastewater treatment, desalination, food processing, medical applications, and pharmaceutical industries. High selectivity, low operating costs, and no pollution charged to the environment make membrane technology an effective tool in urban and industrial water treatment plants [1,2]. UF is a pressure-driven membrane separation process, which uses membranes with pore sizes in the range of 2–100 nm and can filter contaminants larger than 2 nm in size, such as some macromolecules, viruses, bacteria, proteins, and colloidal particles [3,4]. Membrane performance is significantly influenced by the membrane morphology in terms of porosity, pore size and pore size distribution, as well as thickness, which are mainly related to the membrane materials and fabrication techniques [5]. Various types of polymers have been extensively used as the base membrane material in water treatment

* Corresponding author.

Presented at the International Virtual Conference on Water and Energy (ICWE'21), Hassiba Benbouali University of Chlef, Algeria, 25–27 May 2021

technologies. Most of the commercially used polymeric UF membranes are fabricated from polysulfone (PSf), polyethersulfone (PES), polyvinylidene fluoride (PVDF), polyvinyl chloride (PVC), polyacrylonitrile (PAN), and polyethyleneimine (PEI) [6,7]. Polymer type has a significant effect on the filtration performance of the membrane in different ways since each polymer has its own unique features such as degree of polymerization, molecular weight, chain flexibility and chain interactions, which are key factors in determining the overall characteristics of the membrane like thermal, chemical and mechanical properties, as well as filtration performance [4]. A typical asymmetric membrane exhibits a porous dense top layer and a sub-layer which contains large macro voids called finger-like structures. Morphological properties such as porosity, pore interconnectivity, pore geometry, pore size and distribution, homogeneity, macrovoid formation affect the filtration performance of the membranes [8,9]. An ideal membrane is expected to have high water flux, less susceptible to fouling, good selectivity with improved bulk properties such as higher mechanical strength, chemical and thermal stability [10]. Most of the commercial polymeric membranes are produced via phase inversion technique due to its simple processing, flexible production scales, and low cost. There are many factors that affect the pore structure of the phase-inversion membranes, which can be explained not only by ternary diagrams of polymer, solvent and non-solvent but also kinetics, which is much more complicated to control [9,11–13]. Particularly, membrane morphology can be controlled by the choice of polymer, solvent, non-solvent, and preparation parameters for each specific application [14]. Several studies have focused on the investigation of the effect of phase inversion parameters on filtration performance and morphological characteristics of membranes [15–19].

Computational models are gaining importance in design of membrane modules to achieve the best filtration performance with a rapid increase in numerical methods and computational power in recent years. Computational fluid dynamics (CFD) based numerical simulations may provide a detailed description of underlying mechanisms that drive the complex flow through the membrane structure and control the filtration performance of the selected membrane module.

Prediction of flow and fouling based on the membrane geometries and designing membrane modules is a very important design problem. One of the most convenient and cheapest ways to design a whole membrane unit is to create an appropriate model based on modern computational technologies. Understanding the flow through a certain membrane provides necessary data for the optimization of design parameters of the membrane model. Numerical models have been used for the investigation of membrane channel hydrodynamics and their effects on membrane flux with the rapid increase in computational power in the last decade. Ghidossi et al. [20] investigated the effect of physical parameters on the membrane characteristics by using numerical modeling with Ansys Fluent and they obtained pressure and velocity profiles under different operating conditions. Abbasi et al. [21] developed a mathematical model using COMSOL Multiphysics to simulate a full forward-backwash cycle for the ultrafiltration membrane. The model has been validated with the existing experimental data and results were found to be in close agreement. Buetehorn et al. [22] implemented a numerical model using a novel geometry modeling approach to investigate single and multi-phase flows through submerged membrane units with irregular fiber arrangements. Faghihi [23] investigated the effect of different pore shapes on the rejection observed in the membrane filtration and found that the pore geometry was a critical parameter for membrane filtration. It was also reported that triangular and star shaped pores had higher contaminant flux values in comparison to those of other pore shapes. Shi et al. [24] created digital 3D membranes with typical different morphologies having sponge and finger-like structures and investigated their permeabilities using a computational method, which was validated with experimental and empirical results. Even though the porosity was the main parameter that affected the water permeance, membranes with comparable porosities could show different performances due to their morphological properties such as dimension and shape of the finger-like cavities.

The main motivation of this study is to develop a computational model to simulate internal flow structure through the membrane including all physical effects for a realistic simulation of membrane flow. To achieve this, a comprehensive numerical model is developed and validated with the experimental studies conducted in the present study. Finger-like formations were extracted from scanning electron microscopy (SEM) images using an image processing software and included into the numerical model. Internal flow structure inside the porous zone is discussed in detail based on the simulation results.

2. Experimental

2.1. Materials

Polyvinyl chloride (PVC, high molecular weight, *K*-value of 69–71) was used as main membrane polymer, polyethylene glycol (PEG, molecular weight of 6,000 Da) was used as a pore forming agent and N-methyl-2-pyrrolidone (NMP, 99.5% purity) was used as a solvent in the fabrication of membranes.

2.2. Membrane preparation

A PVC based membrane was prepared using phase-inversion with immersion precipitation technique. A casting solution, which consisted of polymer (PVC), pore former (PEG) and solvent (NMP) with different proportions were mixed into a homogenous solution and cast onto a glass plate using an adjustable casting blade followed by immersing into a coagulation bath containing a non-solvent (i.e., water) at 25°C, which resulted in a pore formation due to the exchange between solvent and non-solvent. Membranes were kept in fresh distilled water for 24 h to ensure water soluble components are leached out of the membrane before filtration tests. Membranes were fully dried in a vacuum oven at 50°C for 24 h to remove the humidity prior to characterization (Fig. 1).

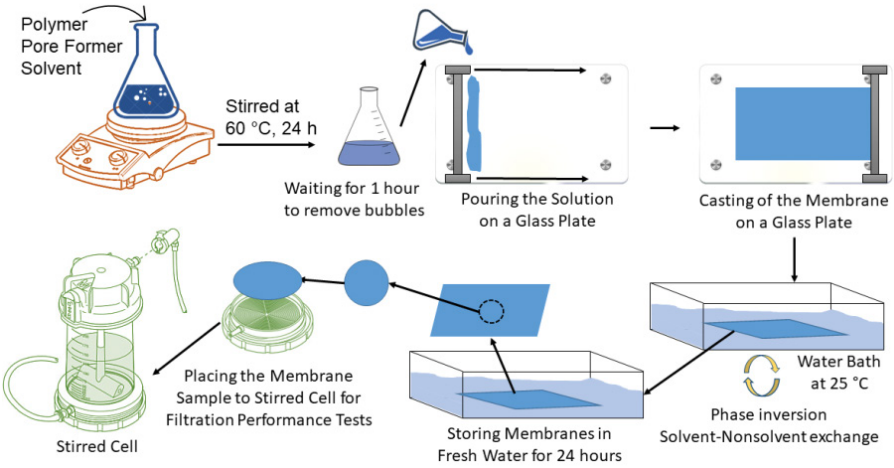

Fig. 1. Membrane preparation steps using phase inversion technique.

2.3. Water flux tests

Water flux of membranes were determined using a dead-end ultrafiltration system. In a typical test, a membrane sample with an effective area of 28.7 cm^2 was placed in a stirred cell of 200 mL and water was introduced into the cell using a compressed nitrogen gas at a constant transmembrane pressure (TMP). Permeate was weighed in one-minute time intervals and the data was collected using a special software supplied by Radwag (Fig. 2). Water flux values were calculated using the following equation for varying TMP of between 0.07 to 0.27 MPa:

$$\text{Water Flux}\left(J_0\right)=\frac{Q}{A\times\Delta t} \tag{1}$$

where J_0 is the water flux (L/m^2 h), Q is the volume of the permeate (L), A is the effective membrane area (m^2) and Δt is the time interval for the measurement (h).

2.4. Scanning electron microscopy imaging and analysis

Cross section images of membranes were monitored by SEM analysis (FESEM, Hitachi, Regulus 8230) at an accelerating voltage of 5–10 kV. Membrane samples were immersed in propyl alcohol and then liquid nitrogen to get them fractured properly. Finger-like formations were included into the model using ImageJ software (National Institutes of Health (NIH, the Laboratory for Optical and Computational Instrumentation (LOCI), University of Wisconsin, ABD) based on the corresponding SEM cross-section images.

2.5. Porosity measurement

Membrane porosity was calculated by the ratio of total pore volume to geometric volume [25]. Membrane sample with a definite area was kept in water until the pores were filled with water and weighed after carefully wiping the surface and the bottom of the membrane. Then, the sample was dried in an oven at 60°C under vacuum to ensure that all the water droplets were removed from the pores since it was demonstrated that even trace amount of water left in the pores would affect the structure of finger-like channels, which in turn would lead to discrepancies in porosity calculation [26]. The well-dried membrane sample was reweighed and the porosity was calculated using the following equation:

$$\varepsilon=\frac{W_{\text{wet}}-W_{\text{dry}}}{\rho_w\times\left(\pi\times r^2\times l\right)}\times 100 \tag{2}$$

where ε is the porosity, W_{wet} and W_{dry} are masses of the wet and dry membranes (g), respectively, ρ_w is the density of water at 25°C (g/cm^3), r is the radius (cm) and l is the thickness of the membrane (cm).

2.5. Numerical modeling of membrane flow

Laminar and incompressible flow through the membrane is described by the following continuity and momentum equations, respectively:

$$\vec{\nabla}\cdot\vec{V}=0 \tag{3}$$

$$\rho\left[\frac{\partial\vec{V}}{\partial t}+\vec{\nabla}\left(\vec{V}\vec{V}\right)\right]=-\vec{\nabla}P+\vec{\nabla}\cdot\left(\mu\vec{\nabla}\vec{V}\right)+\text{SM}_y \tag{4}$$

where ρ is the density of the fluid (kg m^{-3}), $\vec{V}$ is the velocity vector (m s^{-1}), μ is the fluid viscosity (Pa s), P is the pressure (Pa), t is the time (s), and SM_y is a source term in the direction of mean flow through the membrane (kg m^{-2} s^{-2}), which represents resistance by the porous zone to the flow. The pressure drop along the porous zone was modeled using the following Darcy law:

$$S_i=-\left(\frac{\mu}{\alpha}v_i+C_2\frac{1}{2}\rho|v|v_i\right) \tag{5}$$

where S_i and v_i are the source term and velocity component in the i-direction, respectively, α is the permeability

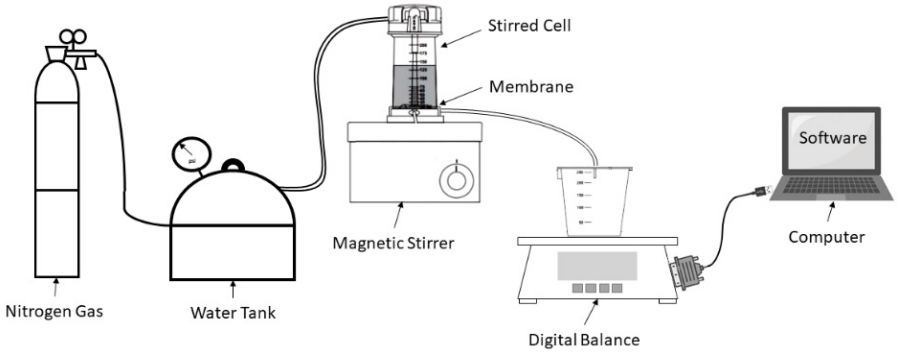

Fig. 2. Schematic view of dead-end ultrafiltration system.

coefficient and C_2 is the inertial resistance coefficient, which was calculated as 3.2×10^{10} from preliminary numerical simulations. The schematic view of the computational domain is shown in Fig. 3 along with the boundary conditions. In order to be consistent with the experimental studies, porosity of the membrane was set to 78.4%, which was determined from the experimental studies using gravimetric method.

Height of the membrane zone in the computational model was selected the same height as in the experimental studies in order to mimic experimental conditions in the numerical model. The length of the inlet zone (h_1) was set to ten times of the membrane height to maintain a fully developed flow field before the membrane zone. The length of the outlet zone (h_2), which coincides at the downstream of the membrane, was selected as ten times of the membrane height to prevent reflection of flow variables at the outlet and to maintain a freestream flow at the downstream of the membrane. Pressure at the inlet was set to a prescribed gauge pressure and the outlet pressure was set to 0 MPa since a freestream flow is formed at the outlet. No-slip boundary conditions were applied for the velocity components at wall boundaries in a viscous flow in order to account wall effects in the simulations. While a uniform rectangular mesh was generated for symmetrical membrane configuration at both inflow and outflow zones, a finer mesh was generated inside the membrane zone in order to capture local changes in the flow field accurately (Fig. 4). The total number of cell in the computational mesh is 48945, which is fine enough to capture present laminar flow through the membrane. Gradient terms were discretized using a least squares cell based method and convection terms were discretized using second-order upwind method in the numerical solution of governing equations. Velocity and pressure equations were coupled using SIMPLE method [27]. Numerical solutions of the governing equations were performed using Ansys Fluent 17.1.

Numerical studies conducted in the present study are two folds. First, a series of numerical simulations are performed for different porosities and pressures to validate the numerical model with the experimental results for symmetrical membrane configuration. In the second-step, in order to elaborate the effect of finger-like structures forming inside the membrane matrix, finger-like geometries were extracted from the SEM image shown in Fig. 5a using an image processing software and extracted irregular geometries were implemented to the background mesh shown in Fig. 4. Then, a triangular unstructured mesh was generated in the second-step of mesh generation procedure to capture outer boundaries of finger-like formations in Fig. 5b, which

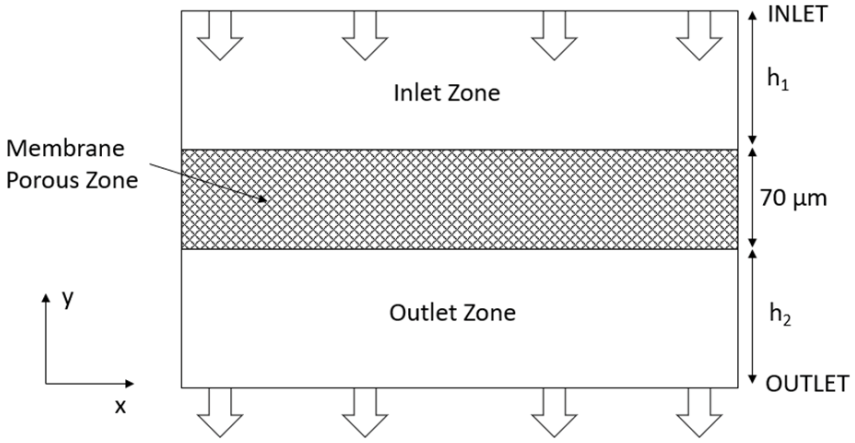

Fig. 3. Schematic view of the computational domain and boundary conditions.

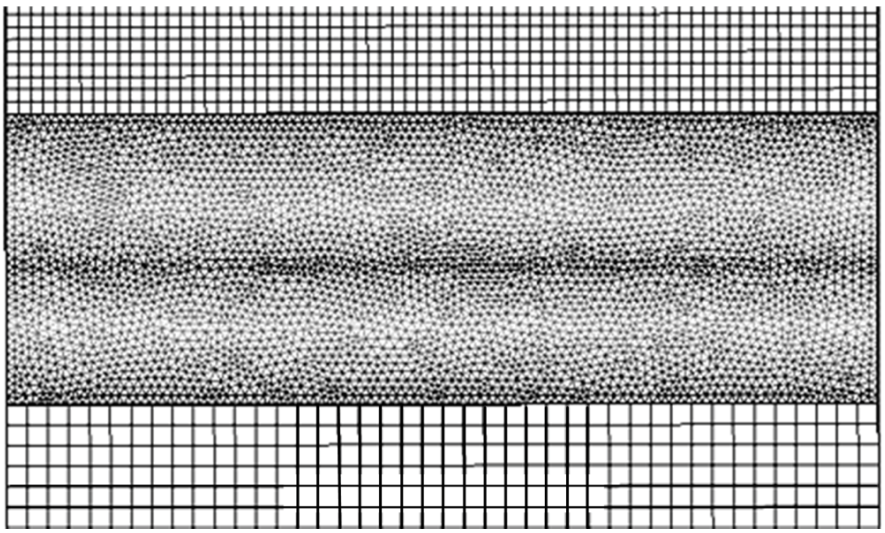

Fig. 4. Unstructured mesh for symmetrical membrane configuration.

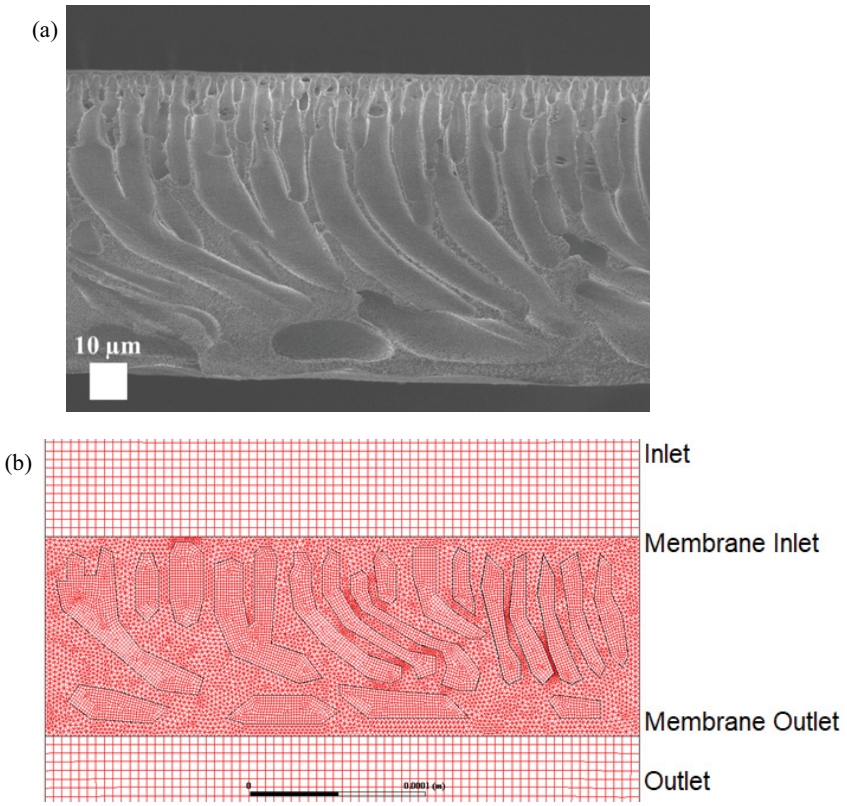

Fig. 5. (a) SEM image and (b) computational mesh for asymmetrical membrane configuration.

is so-called as asymmetrical membrane configuration. Number of cells in the final mesh that contains finger-like structures is 65045 cells.

3. Results and discussion

In order to show the effects of boundary conditions on the numerical results, spatial variations of velocity fields at the inlet and outlet of the membrane are depicted in Fig. 6. The simulated parabolic velocity field at the inlet shows that the inlet boundary conditions could create a fully developed laminar flow. The magnitude of the velocity at the outlet of the membrane significantly decreases due to the inertial resistance inside the porous zones, which proves that the present porosity model can simulate the flow through the porous membrane. The flow entering the membrane zone

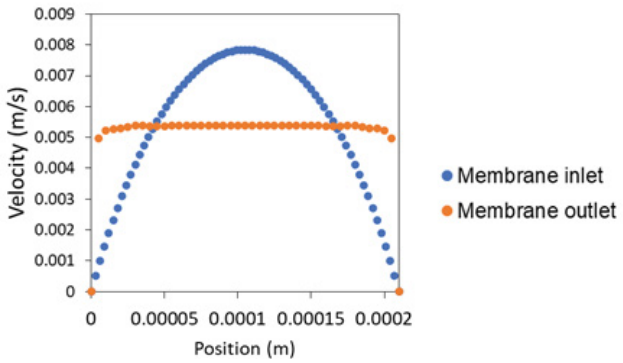

Fig. 6. Velocity profiles at the inlet and outlet of the membrane.

with high momentum may lead to high stresses on the membrane surface.

A series of numerical simulations was performed for a constant porosity of 78.4% using varying inlet pressures and simulated flux values were compared with experimental results in Fig. 7a and b for symmetrical and asymmetrical membrane structures, respectively. Comparison of numerical and experimental results proves that the present computational model is capable of simulating laminar flow through the ultrafiltration membrane used in the experimental studies. While flux tends to increase parabolically with pressure in the experimental results, numerical model predicts a linear relationship between flux and pressure, which may be due to fact that ideal operational conditions prevail in the numerical simulations. As the pores are subjected to significant deformation at high pressures, the measured flux decreases and becomes almost constant when the transmembrane pressure exceeds a certain value. The small discrepancy observed between numerical and experimental results in symmetrical and asymmetrical structures is probably due to the fact that the present numerical model is not sensitive to the pore deformation. Moreover, membrane morphology is assumed to be rigid resulting in larger discrepancies between measured and predicted fluxes for asymmetrical membrane structure than that of symmetrical one [28,29]. This observation reveals that, while performing numerical simulations at high pressures, deformations of pore structures should be considered in the numerical model with the application of fluid-structure interaction, in which fluid and solid equations are strongly coupled spatially and temporally, which is beyond the present study.

The present computational model can be used for the investigation of optimum porosity of an ultrafiltration membrane to yield maximum flux for a prescribed pressure. A series of numerical simulations was performed under 0.07 MPa constant inlet pressure using different porosities in order to see the effect of porosity on the flux performance of UF membrane for symmetrical and symmetrical structures. As seen in Fig. 7c and d, flux values increase linearly with the membrane porosities for both structures. The present

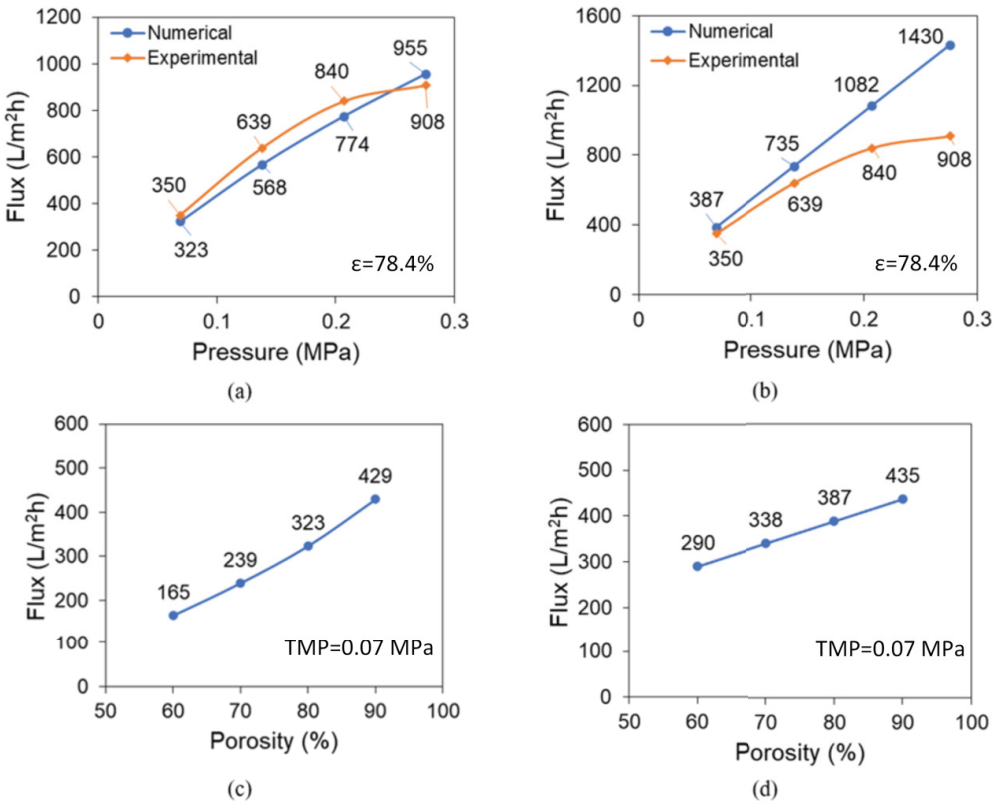

Fig. 7. Comparison of numerical and experimental results for varying inlet pressures (a) for symmetrical, (b) for asymmetrical membrane structure; variation of flux for different porosities (c) for symmetrical and (d) for asymmetrical membrane structure.

numerical model predicted higher flux values in the asymmetrical membrane structure than that in the symmetrical membrane for low porosities due to the fact that the presence of finger-like formations contribute to the permeance significantly as also stated earlier by Lee et al. [30]. However, contribution of the finger-likes becomes less pronounced at high porosities since porosity takes precedence over the finger-like formations and hence permeability is led by the porosity.

Fig. 8 visualizes the internal flow structure inside the membrane zone when finger-like structures are considered in the numerical simulations. A strong momentum exchange is observed between neighboring finger-likes since fluid particles emerging from a finger-like with relatively high momentum penetrates to the neighboring finger-like structures. Penetrating flow through the porous finger-like structures interacts with the internal flow and creates a complex flow structure. This observation proves that the internal flow structure is significantly influenced by the existence of finger-like structures. Increasing flow parcels around finger-like formations may result in recirculation effects and dead zones, which may lead to diminution of flux performance. The flow in the entrance region of the membrane is found to be convectively dominated by the presence of the fingerlikes and becomes a unidirectional flow along the membrane section as the flow approaches to the outlet region of the membrane zone. This observation reveals that the fingerlikes near the entrance section are subjected to significant hydrodynamic effects. A controllable formations of fingerlikes can mitigate such adverse hydrodynamic effects observed at the entrance region by creating more permeable fingerlikes near the upstream.

Pressure contours for asymmetrical membrane configuration is given in Fig. 9.

As seen in the pressure contours visualized in the computational domain, high pressure zones observed at the entrance of the membrane tend to significantly reduce inside the membrane zone due to the energy dissipation over the porous zone. Thus, faces of the fingerlikes close to the entrance of the membrane is subjected to high pressure forces and this may cause a significant deformations at those regions of the fingerlikes, which is consistent with the previous observations in the flow field.

It is known that the addition of hydrophilic nanoparticles into the membrane matrix is able to change the porosity of the membranes by changing the phase inversion rate. For this purpose water flux values of our previous study [31] which has investigated the effect of ZnO addition into membrane matrix, compared with numerical simulations, and the results are given in Fig. 10.

As can be seen in Fig. 10, experimental results above the continuous line depicts the increase of water flux due to the enhancement of membrane morphological properties provided by the presence of ZnO nanoparticles. It is known that water flux is not only related to the pore structure but also with the combined effects of other properties such as hydrophilicity. Agglomeration of the nanoparticles may lead to clogging of pores; therefore the predicted flow can be lower than expected. For 1% and 2% ZnO doped

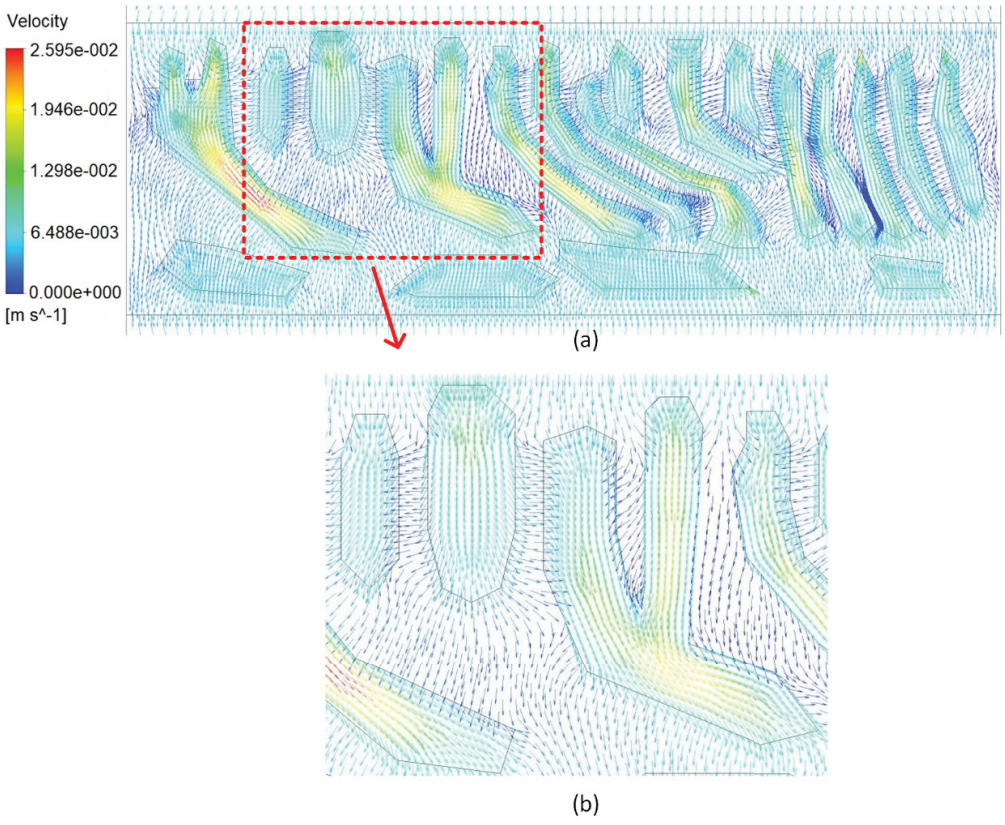

Fig. 8. Velocity vectors of the flow through finger-like structures (a) unzoomed and (b) zoomed views.

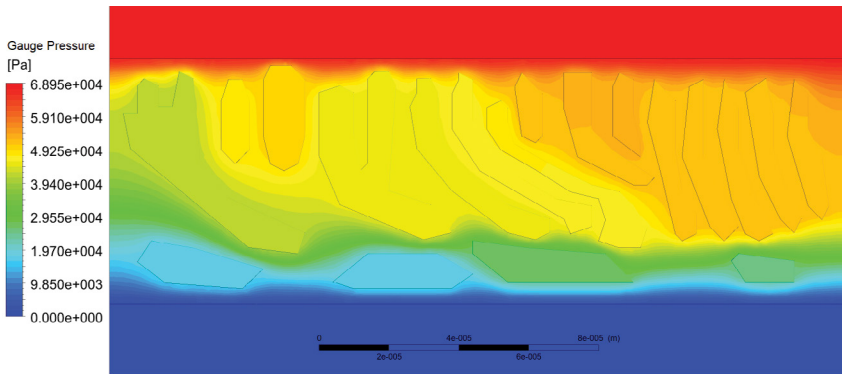

Fig. 9. Pressure contours of the asymmetric membrane.

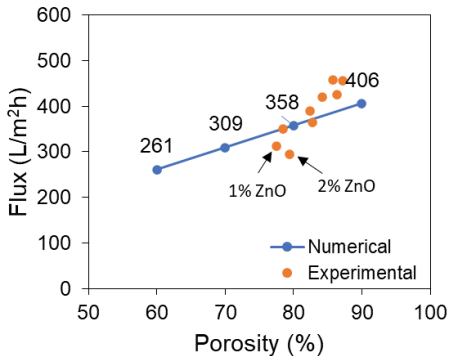

Fig. 10. Flux as a function of porosity for nanocomposite membranes.

membranes, there was significant agglomeration which resulted in clogging of pores with a subsequent reduction in flux.

4. Conclusions

Experimental and numerical studies were carried out for the investigation of the effect of membrane morphology on the flux performance of ultrafiltration membranes. In order to setup and validate the numerical model, phase inversion technique was used for the fabrication of PVC based ultrafiltration membrane and water flux was measured for various transmembrane pressures and pore sizes. Numerical studies were performed for the simulation of flow through the membrane under the same conditions as in the experimental studies. Comparison of numerical and experimental results shows that the present numerical model can accurately predict flux values at low transmembrane pressures. The numerical model overestimated the flux value for high pressures since the present model is not sensitive to the deformation of pore structures. Rigid pore structure assumption used in the present model reduces the accuracy of the numerical results at high transmembrane pressures since pores are subjected to significant deformations at high pressures. In order to assess the effect of finger-like formations on the water flux, finger-like structures were extracted from the SEM images using an image processing software and implemented to the validated numerical model. The simulated velocity vectors inside the membrane zone show that the finger-like structures significantly alter the internal flow structure due to sudden changes in the velocity field around natural formations. Momentum exchange between neighboring finger-likes creates recirculating flow regions, which may result in reduction of the water permeation through the membrane. Finally, finger-like structures can be considered in the numerical simulations using the same methodology described in the present study in order to reveal internal flow structure, which is responsible for the flux performance.

References

[1] K. Konieczny, G. Klomfas, Using activated carbon to improve natural water treatment by porous membranes, Desalination, 147 (2002) 109–116.
[2] O. Al-Abbasi, M.B. Shams, Dynamic CFD modelling of an industrial-scale dead-end ultrafiltration system: full cycle and complete blockage, J. Water Process Eng., 40 (2021) 101887, doi: 10.1016/j.jwpe.2020.101887.
[3] J. Garcia-Ivars, M.-I. Alcaina-Miranda, M.-I. Iborra-Clar, J.-A. Mendoza-Roca, L. Pastor-Alcañiz, Enhancement in hydrophilicity of different polymer phase-inversion ultrafiltration membranes by introducing PEG/Al_2O_3 nanoparticles, Sep. Purif. Technol., 128 (2014) 45–57.
[4] M. Mulder, Basic Principles of Membrane Technology, 2nd ed., Springer Science & Business Media, Germany, 2012.
[5] A. Nqombolo, A. Mpupa, R.M. Moutloali, P.N. Nomngongo, Wastewater Treatment Using Membrane Technology, T. Yonar, Eds., Wastewater and Water Quality, IntechOpen Book Series, 2018, pp. 29–38.
[6] M. Pakbaz, Z. Maghsoud, Performance evaluation of polyvinylchloride/polyacrylonitrile ultrafiltration blend membrane, Iran. Polym. J., 26 (2017) 833–849.
[7] E. Arkhangelsky, A. Duek, V. Gitis, Maximal pore size in UF membranes, J. Membr. Sci., 394 (2012) 89–97.
[8] L. Shen, X. Bian, X. Lu, L. Shi, Z. Liu, L. Chen, Z. Hou, K. Fan, Preparation and characterization of ZnO/polyethersulfone (PES) hybrid membranes, Desalination, 293 (2012) 21–29.
[9] X. Tan, D. Rodrigue, A review on porous polymeric membrane preparation. Part I: production techniques with polysulfone and poly (vinylidene fluoride), Polymers, 11 (2019) 1160, doi: 10.3390/polym11071160.
[10] M.S.S.A. Saraswathi, A. Nagendran, D. Rana, Tailored polymer nanocomposite membranes based on carbon, metal oxide and silicon nanomaterials: a review, J. Mater. Chem. A, 7 (2019) 8723–8745.
[11] H. Strathmann, K. Kock, The formation mechanism of phase inversion membranes, Desalination, 21 (1977) 241–255.
[12] C.A. Smolders, A.J. Reuvers, R.M. Boom, I.M. Wienk, Microstructures in phase-inversion membranes. Part 1. Formation of macrovoids, J. Membr. Sci., 73 (1992) 259–275.

[13] T.H. Young, L.W. Chen, Pore formation mechanism of membranes from phase inversion process, Desalination, 103 (1995) 233–247.
[14] L. Yilmaz, A.J. McHugh, Analysis of nonsolvent–solvent–polymer phase diagrams and their relevance to membrane formation modeling, J. Appl. Polym. Sci., 31 (1986) 997–1018.
[15] J. Xu, Z.L. Xu, Poly(vinyl chloride) (PVC) hollow fiber ultrafiltration membranes prepared from PVC/additives/solvent, J. Membr. Sci., 208 (2002) 203–212.
[16] Q. Alsalhy, S. Algebory, G.M. Alwan, S. Simone, A. Figoli, E. Drioli, Hollow fiber ultrafiltration membranes from poly(vinyl chloride): preparation, morphologies, and properties, Sep. Sci. Technol., 46 (2011) 2199–2210.
[17] S. Hirose, A. Shimizu, T. Nose, Preparation and structures of the poly(vinyl chloride) porous membranes, J. Appl. Polym. Sci., 23 (1979) 3193–3204.
[18] S. Mei, C. Xiao, X. Hu, Preparation of porous PVC membrane via a phase inversion method from PVC/DMAc/water/additives, J. Appl. Polym. Sci., 120 (2011) 557–562.
[19] K.M. Persson, V. Gekas, G. Trägårdh, Study of membrane compaction and its influence on ultrafiltration water permeability, J. Membr. Sci., 100 (1995) 155–162.
[20] R. Ghidossi, J.V. Daurelle, D. Veyret, P. Moulin, Simplified CFD approach of a hollow fiber ultrafiltration system, Chem. Eng. J., 123 (2006) 117–125.
[21] O. Al-Abbasi, M.B. Shams, Transient CFD Modelling of a Full Cycle Dead-End Ultrafiltration Membrane, 2019 8th International Conference on Modeling Simulation and Applied Optimization (ICMSAO), IEEE, Manama, Bahrain, 2019, pp. 1–4.
[22] S. Buetehorn, D. Volmering, K. Vossenkaul, T. Wintgens, M. Wessling, T. Melin, CFD simulation of single- and multi-phase flows through submerged membrane units with irregular fiber arrangement, J. Membr. Sci., 384 (2011) 184–197.
[23] M.H. Faghihi, Effect of Pore Geometry on Membrane Flux Decline Due to Pore Constriction by Particles in Ultra and Micro Filtration (Doctoral Dissertation, Université d'Ottawa/University of Ottawa), 2013.
[24] M. Shi, G. Printsypar, O. Iliev, V.M. Calo, G.L. Amy, S.P. Nunes, Water flow prediction for membranes using 3D simulations with detailed morphology, J. Membr. Sci., 487 (2015) 19–31.
[25] H. Zhao, S. Qiu, L. Wu, L. Zhang, H. Chen, C. Gao, Improving the performance of polyamide reverse osmosis membrane by incorporation of modified multi-walled carbon nanotubes, J. Membr. Sci., 450 (2014) 249–256.
[26] A. Gotzias, The effect of *gme* topology on multicomponent adsorption in zeolitic imidazolate frameworks, Phys. Chem. Chem. Phys., 19 (2017) 871–877.
[27] M.F. Bopape, T.V. Geel, A. Dutta, B.V. der Bruggen, M.S. Onyango, Numerical modelling assisted design of a compact ultrafiltration (UF) flat sheet membrane module, Membranes, 11 (2021) 54, doi: 10.3390/membranes11010054.
[28] E. Demirel, B. Zhang, M. Papakyriakou, X. Shuman, Y. Chen, Fe_2O_3 nanocomposite PVC membrane with enhanced properties and separation performance, J. Membr. Sci., 529 (2017) 170–184.
[29] M.T.M. Pendergast, J.M. Nygaard, A.K. Ghosh, E.M.V. Hoek, Using nanocomposite materials technology to understand and control reverse osmosis membrane compaction, Desalination, 261 (2010) 255–263.
[30] J. Lee, H. Yoon, J.H. Yoo, D.C. Choi, C.H. Nahm, S.H. Lee, H.-R. Chae, Y.H. Kim, C.-H. Lee, P.-K. Park, Influence of the sublayer structure of thin-film composite reverse osmosis membranes on the overall water flux, Environ. Sci. Water Res. Technol., 4 (2018) 1912–1922.
[31] B.M. Erdugan, S. Dadashov, E. Demirel, E. Suvaci, Effect of polymer type on the characteristics of ZnO embedded nanocomposite membranes, Desal. Water Treat., 213 (2021) 159–176.